THE JOURNAL OF BIOLOGICAL CHEMISTRY VOL. 284, NO. 4, pp. 2088–2097, January 23, 2009

Incompatibility with Formin Cdc12p Prevents Human Profilin from Substituting for Fission Yeast Profilin

INSIGHTS FROM CRYSTAL STRUCTURES OF FISSION YEAST PROFILIN[*][S]

Received for publication, September 11, 2008, and in revised form, November 12, 2008 Published, JBC Papers in Press, November 20, 2008, DOI 10.1074/jbc.M807073200

Obidimma C. Ezezika[‡1], Noah S. Younger[§], Jia Lu[¶2], Donald A. Kaiser[¶3], Zachary A. Corbin[‡4], Bradley J. Nolen[‡5], David R. Kovar[§], and Thomas D. Pollard[‡‖6]

From the Departments of [‡]Molecular, Cellular and Developmental Biology and [‖]Cell Biology and Molecular Biophysics and Biochemistry, Yale University, New Haven, Connecticut 06520-8103, the [§]Departments of Molecular Genetics and Cell Biology and Biochemistry and Molecular Biology, The University of Chicago, Chicago, Illinois 60637, and the [¶]Salk Institute for Biological Studies, La Jolla, California 92037

Expression of human profilin-I does not complement the temperature-sensitive *cdc3-124* mutation of the single profilin gene in fission yeast *Schizosaccharomyces pombe*, resulting in death from cytokinesis defects. Human profilin-I and *S. pombe* profilin have similar affinities for actin monomers, the FH1 domain of fission yeast formin Cdc12p and poly-L-proline (Lu, J., and Pollard, T. D. (2001) *Mol. Biol. Cell* 12, 1161–1175), but human profilin-I does not stimulate actin filament elongation by formin Cdc12p like *S. pombe* profilin. Two crystal structures of *S. pombe* profilin and homology models of *S. pombe* profilin bound to actin show how the two profilins bind to identical surfaces on animal and yeast actins even though 75% of the residues on the profilin side of the interaction differ in the two profilins. Overexpression of human profilin-I in fission yeast expressing native profilin also causes cytokinesis defects incompatible with viability. Human profilin-I with the R88E mutation has no detectable affinity for actin and does not have this dominant overexpression phenotype. The Y6D mutation reduces the affinity of human profilin-I for poly-L-proline by 1000-fold, but overexpression of Y6D profilin in fission yeast is lethal. The most likely hypotheses to explain the incompatibility of human profilin-I with Cdc12p are differences in interactions with the proline-rich sequences in the FH1 domain of Cdc12p and wider "wings" that interact with actin.

The small protein profilin not only helps to maintain a cytoplasmic pool of actin monomers ready to elongate actin filament barbed ends (2), but it also binds to type II poly-L-proline helices (3, 4). The actin (5) and poly-L-proline (6–8) binding sites are on opposite sides of the profilin molecule, so profilin can link actin to proline-rich targets. Viability of fission yeast depends independently on profilin binding to both actin and poly-L-proline, although cells survive >10-fold reductions in affinity for either ligand (1).

Fission yeast *Schizosaccharomyces pombe* depend on formin Cdc12p (9, 10) and profilin (11) to assemble actin filaments for the cytokinetic contractile ring. Formins are multidomain proteins that nucleate and assemble unbranched actin filaments (12). Formin FH2 domains form homodimers that can associate processively with the barbed ends of growing actin filaments (13, 14). FH2 dimers slow the elongation of barbed ends (15). Most formin proteins have an FH1 domain linked to the FH2 domain. Binding profilin-actin to multiple polyproline sites in an FH1 domain concentrates actin near the barbed end of an actin filament associated with a formin FH2 homodimer. Actin transfers very rapidly from the FH1 domains onto the filament end (16) allowing profilin to stimulate elongation of the filament (15, 17).

We tested the ability of human (*Homo sapiens*, Hs)[7] profilin-I to complement the temperature-sensitive *cdc3-124* mutation (11) in the single fission yeast profilin gene with the aim of using yeast to characterize human profilin mutations. The failure of expression of Hs profilin-I to complement the *cdc3-124* mutation prompted us to compare human and fission yeast profilins more carefully. We report here a surprising incompatibility of Hs profilin-I with fission yeast formin Cdc12p, a crystal structure of fission yeast profilin, which allowed a detailed comparison with Hs profilin, and mutations that revealed how overexpression of Hs profilin-I compromises the viability of wild-type fission yeast.

EXPERIMENTAL PROCEDURES

Strains, Media, and Chemicals—Kathleen Gould of Vanderbilt University provided strains of *S. pombe*: KYG491, a haploid temperature-sensitive strain with a point mutation in the

* This work was supported, in whole or in part, by National Institutes of Health Grants GM-026338 and GM-066311 (to T. D. P.) and GM-079265 (to D. R. K.). The costs of publication of this article were defrayed in part by the payment of page charges. This article must therefore be hereby marked "*advertisement*" in accordance with 18 U.S.C. Section 1734 solely to indicate this fact.

[S] The on-line version of this article (available at http://www.jbc.org) contains supplemental Figs. S1–S5.

The atomic coordinates and structure factors (codes 3D9Y and 3DAV) have been deposited in the Protein Data Bank, Research Collaboratory for Structural Bioinformatics, Rutgers University, New Brunswick, NJ (http://www.rcsb.org/).

[1] Current address: McLaughlin-Rotman Centre for Global Health, University of Toronto, 101 College St., Toronto, Ontario M5G 1L7, Canada.

[2] Current address: Polaris Pharmaceuticals, Inc., 6370 Nancy Ridge Dr., Suite 106, San Diego, CA 92121.

[3] Current address: Mercenary Lancers, 12484 San Bruno Cove, San Diego, CA 92130.

[4] Current address: J. Philip Kistler MGH Stroke Research Center, 175 Cambridge St., Suite 300, Boston, MA 02114.

[5] Current address: Dept. of Chemistry and Institute of Molecular Biology, University of Oregon, Eugene, OR 97403-1229.

[6] To whom correspondence should be addressed. Tel.: 203-432-3565; Fax: 203-432-6161; E-mail: thomas.pollard@yale.edu.

[7] The abbreviations used are: Hs, *Homo sapiens*; DTT, dithiothreitol; IP_3, inositol 1,4,5-trisphosphate; PDB, Protein Data Bank; r.m.s., root mean square.

S. pombe profilin gene (*cdc3-124 ade6-216 ura4-D18 leu1-32 h*$^+$) and KGY247, a matching wild-type haploid strain (*cdc3+ ade6-216 ura4-D18 leu1-32 h*$^+$). We purchased Edinburgh minimal medium and malt extract media from Bio-101 (Carlsbad, CA), etheno-ATP from Invitrogen, Latrunculin B from Calbiochem (La Jolla, CA), poly-L-proline (M_r 5,000), phloxin-B, thiamine, and nucleotides were from Sigma. We made the poly-L-proline affinity column (18).

Human Profilin Expression in Wild-type and Profilin Temperature-sensitive Strains of S. pombe—We transformed wild-type and profilin temperature-sensitive *cdc3-124* strains of *S. pombe* by electroporation with pREP plasmids carrying Hs profilin-I cDNAs under the control of thiamine-repressible *nmt1*$^+$ promoters. We grew transformed cells at 25 or 36 °C on plates with selective media with 5 mM thiamine to suppress expression or without thiamine to allow expression. Cells were stained with Hoechst dye for fluorescence microscopy.

Protein Purification—We mutated residues of Hs profilin-I on a modified pMW plasmid (19) by PCR (1), verified the changes by sequencing and transformed *Escherichia coli* BL21(DE3) cells for expression and purification (1). Following extraction profilin was bound to a 10-ml affinity chromatography column of poly-L-proline-Sepharose, washed with 3 M urea in Tris-KCl buffer (20 mM Tris-HCl, 150 mM KCl, 0.2 mM DTT, pH 8.0) and eluted with 50 ml of 7 M urea in the same buffer. After refolding profilin during dialysis against 1 mM EDTA, 1 mM DTT, 20 mM Tris-Cl, pH 8.0, gel filtration on a Superdex 75 column in 20 mM Tris-HCl, 150 mM KCl, and 0.2 mM DTT, pH 8.0, produced purified profilin. Peak fractions were pooled, dialyzed *versus* the same buffer in 5–7,000 M_r cut-off tubing and flash frozen. Calcium-ATP actin was prepared from rabbit skeletal muscle (20) and purified by gel filtration on Sephacryl S-300 in G buffer (0.2 mM ATP, 0.5 mM DTT, 0.1 mM $CaCl_2$, 1 mM NaN_3, and 2 mM Tris-Cl, pH 8.0). Polymerized actin was labeled on Cys^{374} with pyrenyl iodoacetamide and monomers were purified by gel filtration (21). Cdc12p FH1 peptides were synthesized by the Keck Center at Yale. We purified from *E. coli* (15) recombinant domains of fission yeast formin Cdc12p consisting of the FH1 domain (Cdc12p(FH1)) or both the FH1 and FH2 domains (Cdc12p(FH1FH2)).

Crystallization and Data Collection—We grew crystals of *S. pombe* profilin using the hanging drop vapor diffusion technique under two different conditions at 4 °C. Approach A used 1 μl of 20 mg/ml of *S. pombe* profilin mixed with 3 μl of crystallization precipitant solution A (1.3 M sodium malonate, pH 7.0, 0.2 M HEPES, pH 7.0, and 0.5% Jeffamine ED2001 (*O*,*O*′-bis-(2-aminopropyl)polyethylene glycol 1900) from Hampton Research (Aliso Viejo, CA). Crystals grew in 5–12 days. Crystals were soaked for 1 min in a cryoprotectant of solution A with 30% glycerol and frozen in liquid nitrogen. Approach B used 1 μl of 13.4 mg/ml *S. pombe* profilin with 3 mM IP_3 mixed with 1 μl of 4 M sodium formate, pH 8.8. Crystals were soaked for 15 s in a cryoprotectant of 4 M sodium formate and 30% glycerol and frozen in liquid nitrogen.

Structure Solution and Refinement—We collected diffraction data (Table 1) from approach A crystals with a diffractometer at the Yale Center for Structural Biology, using a rotating anode x-ray generator at a wavelength of 1.54 Å and 0.1° oscillations. Data were processed and scaled with HKL2000 (22) and yielded a 96.7% complete data set extending to 2.2 Å (Table 1). The program MolRep in the CCP4 suite (23) was used for the molecular replacement using *Acanthamoeba castellanii* profilin-II as the initial model (Protein Data Bank 2ACG). The unit cell contained two monomers. A single round of rigid body refinement was performed in REFMAC (24) followed numerous rounds of positional and isotropic B-factor refinement using REFMAC and manual modeling using COOT (25). This resulted in an $R_{work} \sim 27.8\%$ ($R_{free} = 34.1\%$). Group B factors were refined with TLS (26). The TLS domains were defined using the TLSMD web server for the generation of multi-group TLS models (27). This reduced R_{work} to 24.5% and R_{free} to ~29.4%. ARP/wARP software program in the CCP4 suite (23) identified waters. Subroutines in COOT were used to identify and correct structural problems. A second data set extending to 1.65 Å was collected at beam line X29A of the National Synchrotron Light Source (NSLS) at the National Brookhaven Laboratory using 0.1 oscillations and wavelength of 1.08. These data were used during final rounds of model building and refinement. The final model includes 220 solvent molecules and has an R_{work} of 17.5% and R_{free} of 20.6%. Ramachandran plots indicated that 99% of residues were either in the allowed, favorably allowed, or generously allowed regions (Table 1). The structure validation tool PROCHECK (28) evaluated the geometric quality of the model. We collected data from approach B crystals at Yale and used initial phases from the approach A structure to begin refinement. The final model contained 144 solvent molecules and had an R_{work} of 17.6% and R_{free} of 26.0%. Group B factors were refined with the TLS domains defined using the TLSMD web server (27). Significant drops in R_{work} and R_{free} occurred with TLS refinement. Protein structures were illustrated using the program PYMOL (29) and structural alignments were done with the O program (30).

We made a homology model (see supplemental materials) of the complex of *S. pombe* profilin (PDB 3D9Y) with actin using the structure of bovine profilin-β-actin (PDB 1HLU) as the model. We subjected the initial model to multiple rounds of restrained refinement and structure idealization with standard geometric constraints of bond lengths and angles using the program REFMAC5 in the CCP4 suite. Residues from both chains were refined simultaneously taking into account optimal geometrical orientations of main chain and side chain atoms. We removed steric clashes during structure idealization. Supplemental materials include a PDB file of the homology model.

Biochemical Characterization—Lu and Pollard (1) described the use of intrinsic tryptophan fluorescence to evaluate the stability of profilin in 1 mM EDTA, 1 mM DTT, 20 mM Tris-Cl, pH 8.0, at 22 °C and a range of urea concentrations, and also to quantitate binding of profilin to poly-L-proline and the FH1 domain of Cdc12p. The dissociation equilibrium constant (K_d) was calculated using Kaleidagraph software to fit Equation 1 to the data.

$$F = ((K_d + [L] + [P]) - ((K_d + [L] + [P]) \times 2 - (4[L][P])) \times 0.5)/2[P] \quad \text{(Eq. 1)}$$

F is the relative fluorescence; $[L]$ and $[P]$ are the total concen-

trations of proline and profilin, respectively. Lu and Pollard (1) also described the fluorescence assay to measure dissociation of nucleotide from magnesium-etheno-ATP actin with 0 to 100 μM profilin and spontaneous polymerization of magnesium-ATP-actin monomers (5% pyrene-labeled) in KMEI buffer (10 mM imidazole, 50 mM KCl, 1 mM $MgCl_2$, 1 mM EGTA, pH 7.0). Kovar *et al.* (15) described the use of pyrenyl-actin fluorescence to measure the elongation of actin filaments in the presence of a recombinant *S. pombe* formin Cdc12p(FH1FH2). We used an MCS ITC isothermal titration calorimeter (MicroCal Inc., Northampton, MA) to measure heat changes by interactions of wild-type and mutant profilins with actin monomers at 26 °C. Profilin was concentrated using a Centriprep YM3 concentrator (Millipore Corp., Bedford, MA). Stocks of 20 mM Latrunculin B in ethanol and 10× KMEI were added to both ~25 μM calcium-actin monomers and ~500 μM profilin in buffer G to give concentrations of 50 μM Latrunculin B and 1× KMEI. A 2.0-ml sample of 25 μM actin was in the sample cell and 2.0 ml of buffer was in the reference cell of the ITC unit. With constant mixing by rotation of the injection syringe at 400 rpm, the heat of binding was measured for each addition of 5 or 10 μl of profilin until the actin was saturated with profilin. The small, constant heat of mixing produced at each titration after saturation was subtracted from each of the titration heats and the data were analyzed using MicroCal Origin software to give the stoichiometry (N), the dissociation equilibrium constant (K_d), and the enthalpy (ΔH) for the binding reactions.

RESULTS

Human Profilin-I Does Not Complement the Fission Yeast Profilin cdc3-124 Temperature-sensitive Mutation—We attempted to complement the cytokinesis defect of the temperature-sensitive E42K mutation *cdc3-124* of *S. pombe* profilin by expressing Hs profilin-I from a plasmid under the control of thiamine-repressed, weak Rep81 nmt1 promoter. In the absence of thiamine, this promoter produces profilin concentrations similar to those of the native promoter (1). However, no *nmt* promoter or thiamine concentration tested allowed the *cdc3-124* strain to grow at 36 °C. High level expression of Hs profilin-I from the medium strength Rep3X nmt promoter not only failed to complement the *cdc3-124* mutation, but also killed wild-type fission yeast expressing endogenous levels of wild-type *S. pombe* profilin (Fig. 1). Liquid cultures of cells overexpressing wild-type Hs profilin-I accumulated a proportion of cells with mis-formed septa that eventually lysed starting after 1 day.

The failure of Hs profilin-I to complement the temperature-sensitive mutation and the ability of Hs profilin overexpression to kill wild-type cells were surprising, for many reasons. First, expression of Hs profilin complements deletion of the single profilin gene in *Saccharomyces cerevisiae* (31). Second, expression of fission yeast profilins from this plasmid complements the *cdc3-124* mutation, even expression of the E42K mutant profilin itself or profilin mutants with >90% loss of actin or poly-L-proline binding activity (1). Third, expression of *Arabidopsis* profilin complements the *S. pombe cdc3-124* mutation (32) despite the fact that it lacks nucleotide exchange activity toward actin (33) and thus is less similar to fission yeast profilin (1) than Hs profilin-I (34). Fourth, fission yeast tolerate high level expression of *S. pombe* profilin from the strong Rep3 promoter (1).

Elongation of Actin Filaments with S. pombe Formin Cdc12p—Given these facts and knowledge that fission yeast depend on both profilin and formin Cdc12p to assemble actin filaments for the cytokinetic contractile ring (9–11), we tested the ability of Hs profilin to stimulate the elongation of actin filament barbed ends associated with *S. pombe* formin Cdc12p. The FH2 domain of this formin strongly inhibits elongation of actin filament barbed ends, but *S. pombe* profilin stimulates elongation of Cdc12p constructs having both a profilin-binding FH1 domain and an FH2 domain (15). Remarkably, Hs profilin does not stimulate elongation of barbed ends associated with Cdc12p(FH1FH2) (Fig. 2), despite interacting with both actin monomers and poly-L-proline, the two fundamental ligands thought to be required for this reaction (15, 16). This failure of actin filament elongation likely explains the cytokinesis defects in fission yeast cells dependent on Hs profilin-I. Hs profilin inhibits polymerization in the presence of Cdc12p(FH1FH2) by binding actin monomers and preventing their incorporation at pointed ends and by inhibiting spontaneous nucleation, which contributes a small fraction of the bulk polymerization rates in these experiments.

Crystal Structure of S. pombe Profilin—Seeking an explanation for these unexpected results, we determined two different crystal structures of *S. pombe* profilin (Table 1). One is a 1.65-Å resolution structure (PDB 3D9Y) from crystals formed in 1.3 M sodium malonate, pH 7.0, 0.2 M HEPES, pH 7.0, 0.5% Jeffamine ED2001 (*O*,*O*′-bis(2-aminopropyl)polyethylene glycol 1900). The other is a 2.2-Å resolution structure (PDB 3DAV) from crystals grown in 4 M sodium formate in the presence of IP_3. No density for IP_3 appeared in the electron density map and the two structures are identical. The asymmetric units in both structures contained a dimer of profilin. The dimeric interfaces were different with a contact surface of 310 $Å^2$ for the A structure and 470 $Å^2$ for the B structure. On gel filtration 230 μM *S. pombe* profilin eluted with a Stokes radius of 12.0 Å, similar to the radius of gyration of 13.1 Å calculated from the structure of the monomer using VMD. Thus it is unlikely that the dimer is physiologically relevant.

Despite low sequence identity (Fig. 3*B*) the fold of *S. pombe* profilin (Fig. 3*A*) is remarkably similar to profilins from *S. cerevisiae* (35), mammals (5), and *Acanthamoeba* (36). All of these profilins consist of an anti-parallel β-sheet of six strands flanked by α-helices. The r.m.s. deviation between 125 Cα atoms of *S. pombe* and *S. cerevisiae* profilins is only 1.23 Å, although only 49% of the residues are identical. Residues Gln^4–Thr^{12} of *S. cerevisiae* profilin form a continuous α-helix, whereas an extra residue (Thr^8) in *S. pombe* and *Acanthamoeba* profilins results in residues Gln^4–Ser^9 forming an α-helix followed by residues Leu^{10} to Gly^{13} in a 3_{10}-helix (Fig. 3). A second small difference in architecture is that the loop connecting strand β2 and helix α2 extends further from the core of the protein in *S. pombe* profilin than *S. cerevisiae* profilin. The r.m.s. deviation between corresponding Cα atoms of *S. pombe* profilin and Hs profilin-I is 2.12 Å despite only 33% sequence identity. Human profilins have two small and two large inserts com-

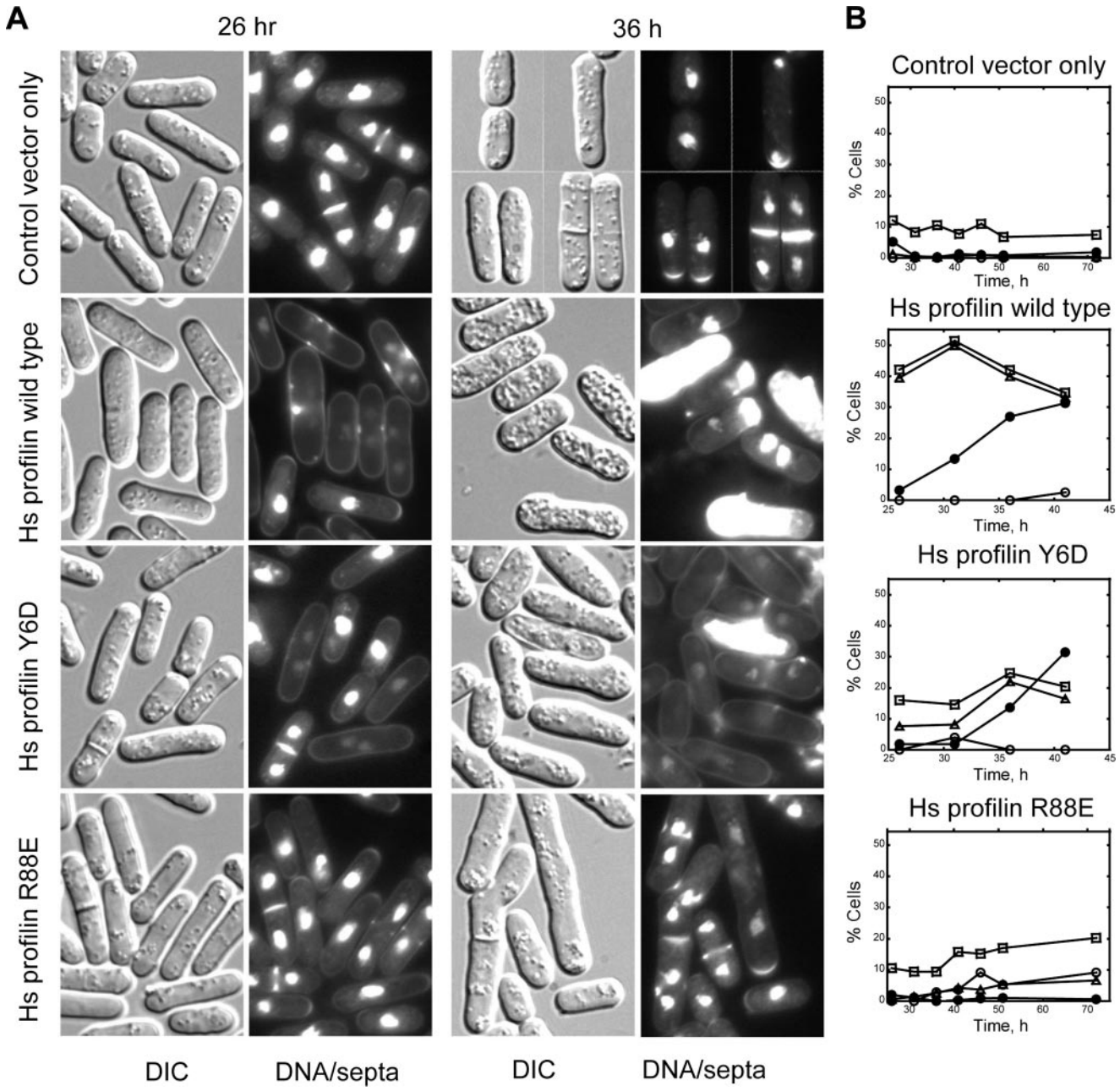

FIGURE 1. **Characterization of fission yeast strains expressing human profilin-I.** Wild-type fission yeast cells transformed with either an empty *pREP3X* plasmid or a *pREP3X* plasmid containing wild-type or mutant Hs profilin-I cDNAs were grown in medium without thiamine to induce expression of Hs profilin-I. *A*, differential interference contrast and fluorescence micrographs of control cells and cells expressing wild-type Hs profilin-I or Hs profilin-I mutants Y6D or R88E. Cells were grown at 25 °C for 26 or 36 h in minimal (Earle's minimal medium) liquid media before staining with Hoechst dye to show nuclei and septa. *B*, distribution of phenotypes over time of expression of profilin-I variants. Symbols: *open squares*, cells with normal septa; *open triangles*, cells with abnormal septa; *open circles*, cells with multiple septa; *filled circles*, lysed cells.

pared with the fungal profilins (Figs. 3*B* and 4). The large insertions extend strands β4, β5 and β6, forming "wings" that flank each side of the actin-binding interface (Fig. 4*B*).

Analysis of Actin Binding Sites—We used a refined homology model (Fig. 4) based on the crystal structure of bovine profilin-β-actin (PDB 1HLU) to examine mutations of *S. pombe* profilin that severely compromise actin binding and fail to complement the temperature-sensitive E42K mutation (*cdc3-124*) or a deletion mutation of the profilin gene (1). Table 2 lists the structural consequences of the mutations having less than 5% wild-type affinity for actin. Steric clashes, loss of intermolecular bonds, or electrostatic repulsion account for most cases of compromised affinity, although the strong effect of the P107Y mutation is not obvious.

Since the divergence of fungi and animals from their common ancestor over 800 million years ago, the actin side and the profilin side of the actin-profilin interface diverged at radically different rates. Today the sequences of *S. pombe* actin and human β-actin are 89% identical and 95% similar. Every residue of bovine β-actin that contacts profilin in the 1HLU crystal structure is identical to the corresponding residue of *S. pombe* actin. On the profilin side of the interface, only 25% of the res-

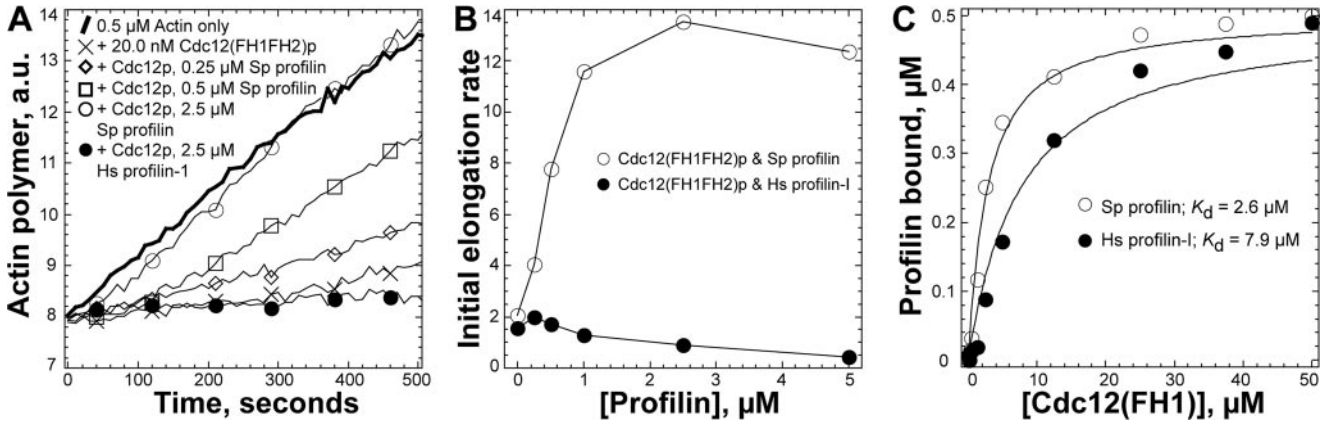

FIGURE 2. **Fission yeast profilin (*S. pombe* PRF), but not human profilin (HPRF), allows Cdc12p-associated actin filaments to elongate their barbed ends.** *A*, effects of profilins and formin Cdc12(FH1FH2)p on the time course of elongation of the barbed ends of preassembled filament seeds. Conditions: 10 mM imidazole, pH 7.0, 50 mM KCl, 1 mM $MgCl_2$, 1 mM EGTA, 0.5 mM DTT, 0.2 mM ATP, 90 μM $CaCl_2$. Reactions were started by mixing 0.5 μM magnesium-ATP actin monomers (10% pyrene labeled) with 0.5 μM actin filaments: *thick curve*, actin alone; other samples contained 20 nM Cdc12(FH1FH2)p with: ×, no profilin; ◇, 0.25 μM *S. pombe* profilin; □, 0.50 μM *S. pombe* profilin; ○, 2.5 μM *S. pombe* profilin; ●, 2.5 μM Hs profilin-I. *B*, dependence of the initial rate of barbed end assembly (slope) with 20 nM Cdc12(FH1FH2)p on the concentrations of (○) *S. pombe* profilin or (●) Hs profilin-I. *C*, affinity of profilin for the Cdc12p proline-rich FH1 domain. Conditions: 20 mM Tris, pH 7.5, 150 mM KCl, 0.2 mM DTT. Either 0.5 μM *S. pombe* profilin (○) or Hs profilin (●) were incubated with a range of concentrations of Cdc12(FH1)p. The intrinsic tryptophan fluorescence of profilin was measured and plotted *versus* the concentration of Cdc12(FH1)p. *Curve* fits revealed the indicated equilibrium dissociation constants.

TABLE 1

Crystal properties, data collection, and refinement statistics for crystals of *S. pombe* profilin

Values in parentheses are for the highest resolution shell.

	S. pombe profilin (PDB 3D9Y)	*S. pombe* profilin (PDB 3DAV)
Crystallization conditions	1.3 M Sodium malonate, pH 7, 0.2 M HEPES, pH 7.0, 0.5% JeffamineED2000	4.0 M Sodium formate, pH 8.8, 3 mM DMyoinositol 1,4,5-trisphosphate
Space group	P1211	P1211
Unit cell dimensions (Å)	a = 36.12 b = 83.58 c = 40.43	a = 35.87 b = 82.42 c = 39.74
Resolution range (Å)	41.78–1.65	41.2–2.20 (2.25–2.20)
Completeness (%)	96.72 (84.22)	96.5 (69.94)
$I/\sigma(I)$	19.3 (2.2)	15.2 (4.0)
Redundancy	2.8 (1.9)	2.9 (2.2)
R_{merge} (%)	3.9 (2.5)	9.0 (34.0)
Refinement statistics		
R_{cryst}, %[a]	17.5 (24.7)	17.6 (23.3)
R_{free}, %[b]	20.6 (23.9)	26.0 (29.5)
Bond length r.m.s. deviation (Å)	0.009	0.008
Bond angles r.m.s. deviation	1.256	1.146
Mean B value	15.22	24.06
Water molecules	220	143
Ramachandran plot statistics (%)		
Most favored	93.8	91.8
Additionally allowed	5.2	7.7
Generously	0	0
Disallowed	1.0	1.0

[a] $R_{cryst} = \Sigma(F_o - F_c)/\Sigma(F_o)$.
[b] $R_{free} = \Sigma(F_o - F_c)/(F_o)$ for 5% of data not used in refinement.

idues of bovine profilin that contact actin in the 1HLU structure are identical to the corresponding residues of *S. pombe* profilin (Fig. 3*B*). Remarkably, despite extensive differences (Table 3), fission yeast and bovine profilins have the same affinity for rabbit muscle actin (K_d = 0.1–0.2 μM) in fluorescence quenching and nucleotide exchange assays (1, 37, 38). The seven identical residues that interact with actin in human and *S. pombe* profilins have similar conformations in the two profilin structures. Four of the identical residues (Arg^{72}/Arg^{74}, *S. pombe* profilin/Hs profilin, Gly^{108}/Gly^{121}, Lys^{112}/Lys^{125}, Ser^{77}/Ser^{84}) make hydrogen bonds with actin. Profilin residue Ile^{71}/Ile^{73} makes important hydrophobic interactions with Leu^{171} and Pro^{172} of actin. Conserved profilin residue Lys^{67}/Lys^{69} forms two salt bridges with actin. Highly conserved residue profilin Gly^{60}/Gly^{62} does not interact with actin but may be important for the conformation of the loop between helix α3 and strand β3.

Residues in the interface with actin that differ between human and *S. pombe* profilins appear to provide Hs profilin with more interactions with actin than *S. pombe* profilin (Table 3), so other interactions must compensate. We note three examples of possible compensation. (i) *S. pombe* profilin lacks the salt bridges formed by Glu^{82} and Lys^{90} in the wings of Hs profilin that extend around the barbed end of actin, but Lys^{84} on the shorter β5/β6 loop compensates by forming a salt bridge with actin Glu^{167}, which is not available to the homologous residue Thr^{97} of Hs profilin. The residue corresponding to *S. pombe* profilin Lys^{84} is alanine in *S. cerevisiae* profilin, and the absence of this salt bridge may contribute to the lower affinity (K_d = 2.9 μM) of *S. cerevisiae* profilin for muscle actin (35). (ii) Two extra residues make helix α2 of *S. pombe* and *S. cerevisiae* profilins a half-turn longer than human profilins and move helix α3 so that it interacts differently with actin (Fig. 4*A*). The position of *S. pombe* helix α3 optimizes hydrophobic interactions of profilin side chain of Phe^{57} with the backbone and side chains of actin Leu^{170} and His^{173}, but precludes other interactions such as the interaction of Hs profilin residue Val^{60} at the end of helix α3 with actin Val^{287}. The homologous residue Gly^{58} of *S. pombe* profilin is too distant to interact with actin. (iii) Differences in the conformations of the β7-α4 loops of yeast and human profilins may influence interactions with helix αM in subdomain 1 near the C terminus of actin (Fig. 4). His^{119} in this loop of Hs profilin hydrogen bonds with the hydroxyl group of Tyr^{169}. The *S. pombe* profilin residue homologous to His^{119} is Leu^{106}, which is oriented differently and makes neither ionic interactions with actin nor fills the space occupied by bovine His^{119}.

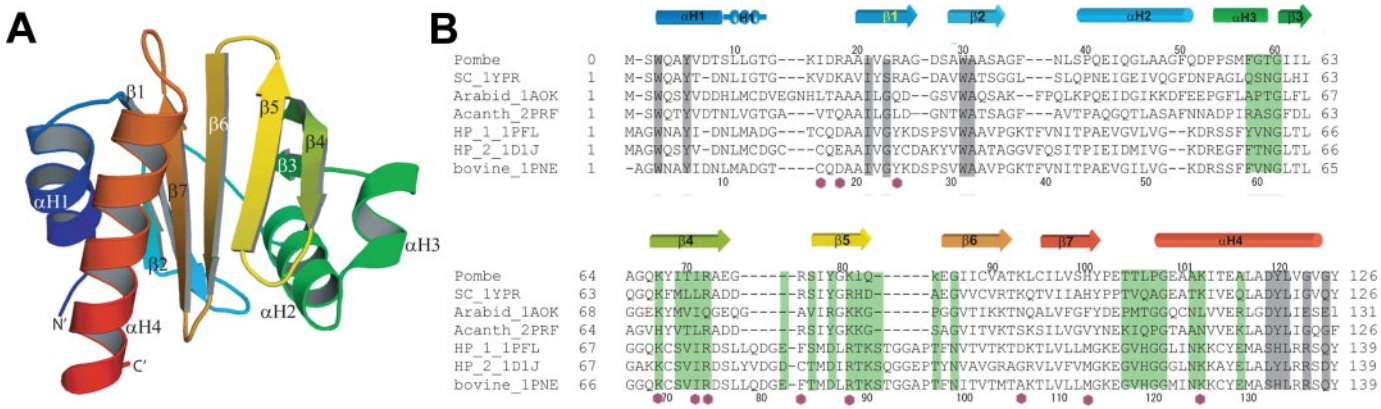

FIGURE 3. **Structure of fission yeast profilin.** *A*, ribbon diagram of *S. pombe* profilin showing the secondary structure with the four helices labeled αH1–αH4 and seven β-strands labeled β1–β7. *B*, comparison of profilin sequences aligned based on crystal structures with α-helices noted as *cylinders*, β-strands noted as *arrows*, and residues implicated by mutagenesis in phosphatidylinositol 4,5-bisphosphate binding noted with *purple circles*. *SC*, *S. cerevisiae* profilin (PDB 1YPR); *Arabid*, *Arabidopsis thaliana* profilin (PDB 1AOK); *Acanth*, *A. castellanii* profilin (PDB 2PRF); HP_1, Hs profilin-I (PDB 1PFL); HP_2, Hs profilin-II (1DIJ); and bovine profilin (PDB 1PNE). Structural alignments were done with the O program. Highlights show residues that interact with actin (*green*) or polyproline (*gray*) in crystal structures. Residue numbers for *S. pombe* profilin are shown *above* the sequences, whereas those of bovine profilin are shown *below* the sequence alignment.

*Comparison of Poly-*L*-proline Binding Sites*—*S. pombe* profilin binds poly-L-proline with a 5-fold higher affinity (K_d = 55 μM proline residues; (1)) than Hs profilin (K_d = 200–300 μM proline residues) (39). Similarly *S. pombe* profilin had a higher affinity for Cdc12p(FH1) (K_d = 2.6 μM) than Hs profilin-I (K_d = 7.9 μM) (Fig. 2*C*). Most of the 11 residues constituting the poly-L-proline binding site of *S. pombe* profilin are identical in other profilins (Fig. 3). Conserved aromatic side chains of Trp^3, Tyr^6, and Tyr^{31} stack upon each other in a linear array between the N- and C-terminal helices. Other features must account for the higher affinity of *S. pombe* profilin for poly-L-proline and Cdc12(FH1)p. One candidate is Tyr^{120}, a fourth aromatic residue in this groove of *S. pombe* profilin in place of histidine in this position in Hs profilin-I and bovine profilin. Another difference is glycine in the penultimate position of *S. pombe* profilin and Hs profilin-II *versus* glutamine in Hs profilin-I and budding yeast profilin. Both molecules in *S. pombe* profilin crystals grown in sodium malonate have electron density in the polyproline binding site, which we modeled as glycerol molecules located within hydrogen bonding distances to Met^1, Trp^3, and/or Trp^{31}.

We attempted to determine the structure of *S. pombe* profilin with bound proline-rich peptides from the FH1 domain of *S. pombe* formin Cdc12p, an important ligand for profilin in these cells. We tested two peptides: Cdc12p-(905–915) (PTPPPPPPLPVK) and Cdc12p-(942–956) (PAFPPPPPPPPPLVS). No density for Cdc12p-(905–915) appeared in maps from crystals soaked in 6 mM peptide for 45 h. We also co-crystallized profilin with 5 mM Cdc12p-(942–956) by approach A but did not observe any peptide density.

Comparison of Polyphosphoinositide Binding Sites—Experiments on mammalian profilins implicated two sites in interactions with phosphatidylinositol 4,5-bisphosphate (Fig. 3*B*). One site is near the polyproline binding site and the other partially overlaps the actin binding site (40). Of these 11 candidate residues, 7 differ between human and fission yeast profilins, giving the yeast profilin a net positive charge at these sites of +8.5 compared with +3 for Hs profilin-I. No information is available on the affinity of *S. pombe* profilin for phosphatidylinositol 4,5-bisphosphate, but this difference encouraged us to co-crystallize *S. pombe* profilin with IP_3. Co-crystallization of *S. pombe* profilin with IP_3 by approach B produced crystals that diffracted to 2.2 Å but the maps showed no electron density for IP_3.

Characterization of Human Profilin-I Mutants with Loss of Ligand Binding Activities—To learn which interactions contribute to the ability of Hs profilin-I to kill fission yeast, we designed point mutations to compromise interactions with actin or poly-L-proline or catalyze nucleotide exchange. To disrupt poly-L-proline binding, we focused on Hs profilin residue Tyr^6, because mutations of the homologous Tyr^5 of fission yeast profilin can lower the affinity for poly-L-proline 100-fold (1). To interfere with actin binding we mutated Arg^{88}, because mutation of Lys^{81} at this position in fission yeast profilin to glutamic acid reduced the affinity for actin nearly 100-fold (1). We compared these new mutant profilins with two mutant profilins used in previous studies, H119E profilin, a mutation in the actin binding site (41); and H133S profilin, a mutation in the poly-L-proline binding site (42). The biochemical properties of our new mutant profilins have not been published, although we used them to characterize profilin interactions (15).

We purified human profilins from *E. coli*, tested their stability, and measured their affinities for actin and poly-L-proline (Table 4). We used intrinsic tryptophan fluorescence to measure denaturation of profilin over a range of urea concentrations. The midpoint in the transition between the native and denatured states occurred at 3.7 M urea for wild-type Hs profilin-I. The least stable mutant, Y6D profilin, denatured with a midpoint at 2.6 M urea. The denaturation midpoints of all other mutant profilins were 2.9 M urea or higher. We did not test Hs profilin-I R88E, but note that it binds poly-L-proline with the same affinity as wild-type profilin, evidence that it folds correctly.

We used the increase of intrinsic tryptophan fluorescence emission (38, 43) to measure binding of poly-L-proline to profilins (supplemental Fig. S1). The affinity of Y6D profilin for poly-L-proline was 1200-fold lower than wild-type profilin and 28 times lower than H133S profilin (Table 4), the mutant profilin used most often in biological experiments (for example, see

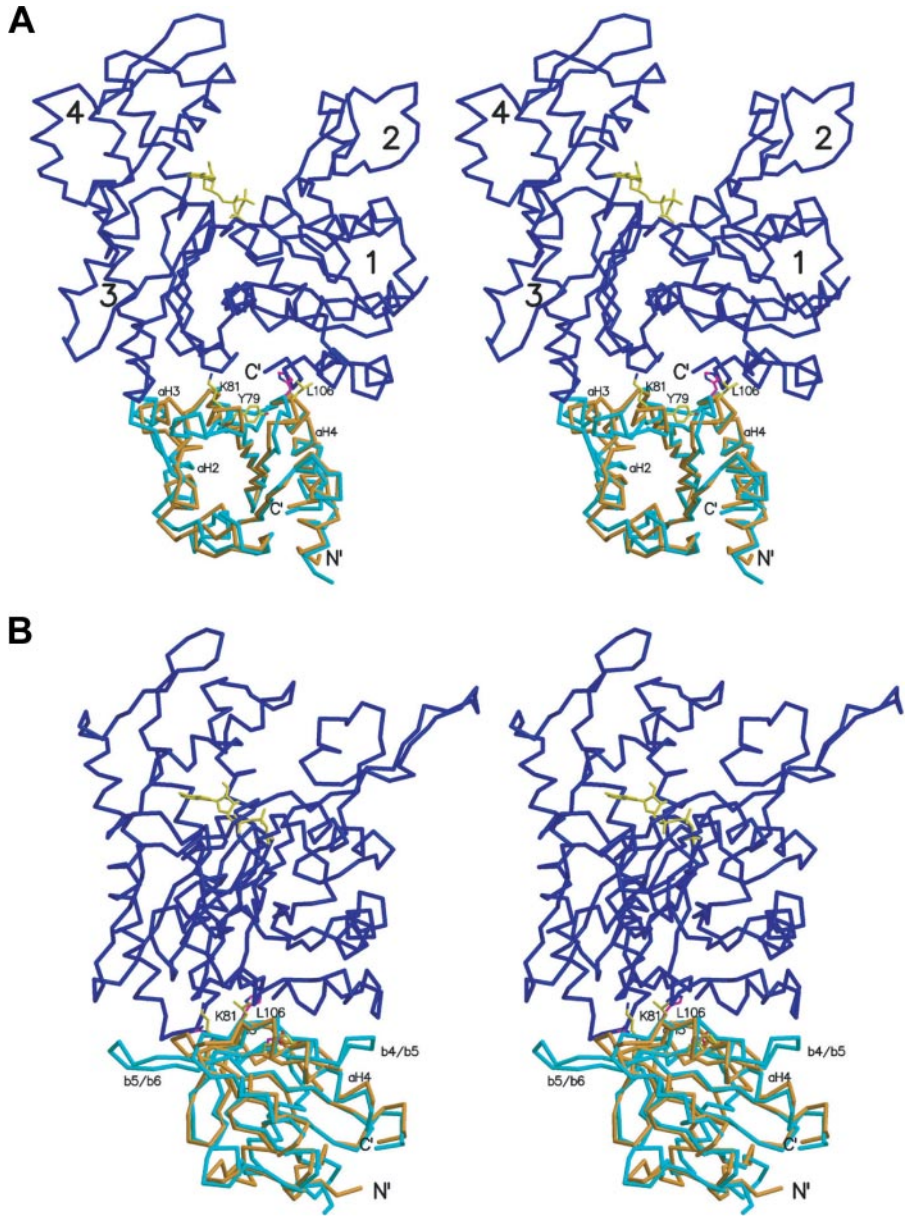

FIGURE 4. **Stereo diagrams of the homology model of *S. pombe* profilin bound to actin based on the bovine profilin-β actin crystal structure (PDB 1HLU).** Color code for C-α traces: actin, *dark blue*; bovine profilin, *cyan*; *S. pombe* profilin, *tan*. ATP is *yellow*. Some residues discussed in the text are shown in stick representation. Subdomains 1–4 of actin are labeled in *panel A*. Important secondary structural elements are also labeled. The figure in *panel B* is oriented to highlight the β4/β5 and β5/β6 wings in bovine profilin. The figure was generated using Molscript and Raster3D.

Ref. 44). The affinities of other mutant profilins for poly-L-proline were not significantly different from wild-type profilin (Table 4).

Isothermal titration calorimetry (Fig. S2) in a low salt buffer or 50 mM KCl, 1 mM $MgCl_2$ with Latrunculin B to inhibit polymerization showed that the H119E mutation (41) reduced affinity for actin about 25-fold. We detected no heat change when titrating R88E profilin into actin either in buffer G or in KCl with Latrunculin B, so it did not bind at concentrations up to 175 μM. Inhibition of spontaneous polymerization requires 8–20 times more H119E profilin than wild-type profilin, but R88E profilin did not inhibit polymerization at concentrations as high as 100 μM (supplemental Fig. S3).

We measured the time course of dissociation of etheno-ATP from monomeric actin in excess unlabeled ATP as a second assay of the affinity of profilin for actin and to measure the maximal enhancement of nucleotide exchange (supplemental Fig. S4). The dependence of k_{obs} on profilin concentration gave K_d values of 0.34 μM for H119E profilin-I. Saturating H119E profilin-I dissociated etheno-ATP at less than half the rate of wild-type profilin (supplemental Fig. S4). Concentrations of R88E profilin up to 100 μM had no effect on nucleotide exchange, indicating that the K_d is $>$100 μM. We attempted to modify the nucleotide exchange activity of Hs profilin with substitutions for Asp^{86} (data not shown). The D86R substitution reduced the affinity for actin and the maximum nucleotide exchange rate 4–5-fold, whereas the D86N substitution increased both the affinity for actin and the maximum rate of nucleotide exchange 2–3-fold. Profilins D86A, D86L, and D86Y were similar to wild-type Hs profilin-I.

Characterization of the Human Profilin Overexpression Phenotype in Fission Yeast—The ability of Hs profilin-I overexpression to compromise the viability of wild-type fission yeast allowed us to test which interactions of profilin are important for this dominant phenotype (Figs. 1 and supplemental S5). Overexpression of wild-type Hs profilin-I for 1 day produced many cells with abnormal septa, and lysed cells accumulated after 20 h. Overexpression of mutant Y6D (that binds actin but not poly-L-proline) also killed fission yeast, but lysis did not begin until about 30 h and fewer cells had abnormal septa than cells overexpressing wild-type Hs profilin-I. Overexpression of human profilins with substitutions for Asp^{86} also killed wild-type cells (supplemental Fig. S5). On the other hand, fission yeast overexpressing Hs profilin-I mutants R88E (with no detectable affinity for actin) or H119E (with affinity for actin reduced 10-fold) were viable, although the cultures had a few more cells with multiple or abnormal septa than control cultures.

DISCUSSION

Divergence of the Profilin Side of the Profilin-Actin Interface—Since the divergence of fungi and animals more than 800 mil-

TABLE 2

Analysis of *S. pombe* profilin mutations that failed to complement profilin temperature-sensitive and/or profilin null strains

Residue	Native interaction with actin	Mutation	Affinity for actin[a]	Consequence of mutation
Lys^{67}	Side chain salt bridges to actin Asp^{287} and Asp^{285}	K67A	<0.01	Loss of salt bridge
		K67E	<0.01	Loss of salt bridge and electrostatic repulsion
Ile^{71}	Hydrophobic interaction of side chain with actin	I71E	<0.01	Intramolecular salt bridge with profilin Lys^{81} precludes interaction with actin
		I71R	<0.01	Steric hindrance and charged side chain in hydrophobic cavity
		I71W	<0.01	Steric clash
Arg^{72}	Side chain salt bridge to actin Phe^{374} C-terminal carboxyl	R72E	Not tested	Disrupts network of salt bridges including actin C terminus
Tyr^{79}	Tyr^{79} OH makes potential H bond to actin Glu^{115} side chain	Y79R	0.053	Arg^{79} side chain forms salt bridge to actin Phe^{374} C terminus; may compromise network of native electrostatic bonds
Lys^{81}	Side chain H bonds to carbonyl O's of actin Glu^{166} and Tyr^{165}	K81E	<0.01	Loss of 2 H bonds
Pro^{107}	Side chain between side chains of actin Tyr^{168} and profilin Tyr^{101}	P107W	0.04	Steric clash of large side chain with actin side chains; displaces side chains and backbone in refinement
		P107Y	0.055	Small steric clashes; mechanism not clear
Ala^{111}	Small side chain in water-filled cavity near actin C terminus	A111E	0.023	Electrostatic repulsion between Glu^{111} side chain and actin Phe^{374} C-terminal carboxyl

[a] Data from Lu and Pollard (1).

TABLE 3

Contacts between homologous residues of human and *S. pombe* profilins and actin in the bovine profilin-β-actin complex (PDB code 2BTF) and *S. pombe* profilin-actin homology model

Surface contacts were computed using CCP4 program suite and checked with Swiss PDB Viewer. Donor and acceptor atoms separated <3.3 Å with acceptable geometry were defined as hydrogen bonds.

Human	*S. pombe*	Interactions between profilin and actin	Δ[a]
Phe^{59}	Phe^{57}	Side chains stack below actin His^{173}	0
Val^{60}	Gly^{58}	Val^{60} carbonyl O H-bonds to amide N of actin Val^{287}. Position of α3 precludes this bond for Gly^{58}	+1
Lys^{69}	Lys^{67}	Both make potential salt bridges to actin Asp^{288} side chain	0
Ser^{71}	Ile^{69}	Ser^{71} side chain H-bonds with actin Asp^{286} side chain. Ile^{69} side chain makes hydrophobic contact	0
Ile^{73}	Ile^{71}	Side chains make hydrophobic contacts with actin	0
Arg^{74}	Arg^{72}	Side chains make potential salt bridge to actin Phe^{375} C-terminal carboxyl	0
Ser^{76}	Glu^{74}	Ser^{76} no actin contact. Glu^{74} side chain can make salt bridge to actin Lys^{113} or Arg^{372} side chains	−1
Gln^{79}	None[b]	Gln^{79} side chain might make H-bond with side chain of actin Lys^{113}	+1
Glu^{82}	None[b]	Side chain of Glu^{82} may form a salt bridge to actin Lys^{113} side chain	+1
Thr^{84}	Ser^{77}	Side chains make hydrogen bonds to actin Arg^{372} side chain	0
Asp^{86}	Tyr^{79}	Asp^{86} side chain repelled by actin Phe^{375} C-terminal carboxyl. Tyr^{79} side chain has room	−1
Arg^{88}	Lys^{81}	Arg^{88} side chain makes salt bridge to actin Glu^{167} side chain. Lys^{81} side chain makes H-bonds to carbonyl O's of actin Tyr^{165} and Glu^{166}	−1
Lys^{90}	None[b]	Lys^{90} forms salt bridges with actin Asp^{286} and Asp^{288} side chains	+2
Thr^{97}	Lys^{84}	Thr^{97} makes potential H-bond with Glu^{167} side chain. Lys^{84} forms salt bridge with actin Glu^{167} side chain	0
Asn^{99}	Gly^{86}	Asn^{99} side chain makes non-ideal H-bond to actin Tyr^{169} side chain OH. Gly^{86} makes no contacts	+1
His^{119}	Leu^{106}	His^{119} side chain makes non-ideal H-bond to actin Tyr^{169} side chain OH. Both His^{119} and Leu^{106} contact Met^{355}	(+1)
Gly^{120}	Pro^{107}	Gly^{120} amide makes H bond with Tyr^{169} side chain OH. Pro^{107} contacts actin Tyr^{169}	0
Gly^{121}	Gly^{108}	Gly^{121} amide makes non-ideal H bond to actin Phe^{375} carboxyl. Gly^{108} has no contact	(+1)
Asn^{124}	Ala^{111}	Asn^{124} side chain makes H bond with Arg^{372} side chain εN. Ala^{111} makes no contact	+1
Lys^{125}	Lys^{112}	Lys^{125} makes salt bridge to actin Glu^{361} side chain and if rotated to Glu^{364} side chain. Lys^{112} makes long H-bonds with carbonyl O's of actin Gln^{354} and Met^{355}	0

[a] Δ is number of Hs profilin-I interactions with actin minus the number of *S. pombe* profilin interactions with actin.
[b] *S. pombe* profilin lacks homologous residues on the wings of Hs profilin-I.

lion years ago, evolution has shaped the two sides of the actin-profilin interface differently. Every residue on the actin side of this interface is identical in humans and fission yeast, so strong selective pressures on actin must have maintained the ancestral structure on both phylogenetic branches since that time. These pressures may include interactions with other proteins, because genome-wide analysis indicates that the surfaces of proteins with multiple protein interactions evolve more slowly than proteins with few interactions (45). The profilin binding site on actin may be an extreme case, because the groove between subdomains 1 and 3 forms overlapping binding sites for profilin and several other proteins (46). We do not know the structure of the ancestral profilin, but amino acid substitutions on the conserved profilin backbone framework created surfaces on human and *S. pombe* profilin that bind actin with the same affinity despite the fact that only 7 of the 24 homologous residues are identical (Fig. 2*B*). Of the differences only two are conservative substitutions. This divergence in the actin binding sites may have functional consequences, such as fine tuning isoform-specific interactions of profilins with formins.[8]

Why Does Human Profilin Fail to Substitute for S. pombe Profilin in Vivo?—Hs profilin-I neither complements the temperature-sensitive *cdc3-124* mutation in *S. pombe* profilin nor stimulates elongation of filaments of vertebrate muscle actin associated with *S. pombe* formin Cdc12p. The profilin binding

[8] Neidt, E. M., Scott, B. J., and Kovar, D. R. (2009) *J. Biol. Chem.* **284,** 673–684.

TABLE 4
Properties of human profilin-I mutants

Profilin type	Urea stability	Poly-L-proline binding	Actin binding by ITC in low salt buffer	Actin binding by ITC in KCl, Mg, Lat B	Actin binding by nucleotide exchange	Actin nucleotide dissociation rate	Fission yeast over expression phenotype
	M	*K_d, mM proline residues*	*K_d μM, ΔH cal*	*K_d μM, ΔH cal, stoichiometry*	*K_d μM*	*s^{-1}*	
Wild type	3.7	0.40–0.49	0.15, −5000	0.02, −4800, 0.85	0.1	0.24	Dead
H119E	3.7	0.43–0.56	4.1, −3500		4.2–20	0.04	Alive
R88E	ND[a]	0.45–0.65	No heat change	No heat change	No activity	No activity	Alive
H133S	3.2	20.1		0.06, −6560, 0.84	ND	ND	Dead
Y6D	2.5	564		0.09, −5560, 0.84	ND	ND	Dead

[a] ND, not determined.

sites on vertebrate muscle actin and *S. pombe* actin are identical, but we recognize that further experiments with fission yeast actin might reveal additional biochemical differences. Because cytokinesis in fission yeast requires Cdc12p (9) and profilin (11), the failure of Hs profilin-I to substitute for *S. pombe* profilin is likely due to the strong dependence of Cdc12p on profilin for actin polymerization (15). We do not yet understand why Hs profilin fails to support actin filament elongation by Cdc12p, but three differences between these profilins might contribute. One is the lower affinity of Hs profilin for the FH1 domain of Cdc12p. This binding reaction is rate-limiting for elongation of actin filaments by formins such as Cdc12p that strongly inhibit actin filament elongation in the absence of profilin (16, 47). The second difference is the presence of wider wings on Hs profilin formed by 10 extra residues not present is fission yeast profilin (Fig. 4). These wings may interfere with actin filament elongation by Cdc12p. A third difference is that the region of profilin proposed to bind polyphosphoinositides is more strongly positive in fission yeast profilin than Hs profilin-I. Further biochemical experiments will be required to learn which of these or other differences explain the lack of function of Hs profilin in fission yeast and the incompatibility between Hs profilin and *S. pombe* formin Cdc12p.[9]

Our observations emphasize that formin Cdc12p is the key polyproline ligand for profilin in fission yeast (9). In contrast, Hs profilin-I can complement deletion of the single profilin gene in *S. cerevisiae* (31). A possible explanation is that the budding yeast formin Bni1p does not inhibit barbed end elongation as strongly as Cdc12p, so neither this formin nor cytokinesis in budding yeast is as dependent on profilin as *S. pombe* and Cdc12p.

Why Is Overexpression of Hs Profilin-I Lethal to S. pombe?—Human profilins that bind actin with wild-type affinity kill *S. pombe* regardless of their ability to bind poly-L-proline. Human profilins with affinity for actin reduced by 10-fold by the H119E mutation or >100-fold by the R88E mutation do not have this dominant overexpression phenotype. We cannot evaluate the impact of nucleotide exchange on this phenotype, because two mutants with low nucleotide exchange activity, H119E and D86R, also have lower affinity for actin.

Partial occupancy of the cellular actin monomer pool by Hs profilin will slow or stop assembly of actin filaments for the contractile ring in direct proportion to the depletion of the pool of monomeric actin bound to *S. pombe* profilin. Depletion of actin competent to polymerize filaments for the contractile ring can explain the observed defects in cytokinesis and septation.

Acknowledgments—We thank K. S. Pollard and D. A. Pollard for helpful suggestions.

REFERENCES

1. Lu, J., and Pollard, T. D. (2001) *Mol. Biol. Cell* **12,** 1161–1175
2. Pollard, T. D., Blanchoin, L., and Mullins, R. D. (2000) *Annu. Rev. Biophys. Biomol. Struct.* **29,** 545–576
3. Tuderman, L., Kuutti, E.-R., and Kivirkko, K. (1975) *Eur. J. Biochem.* **52,** 9–16
4. Tanaka, M., and Shibata, H. (1985) *Eur. J. Biochem.* **151,** 291–297
5. Schutt, C. E., Myslik, J. C., Rozycki, M. D., Goonesekere, N. C., and Lindberg, U. (1993) *Nature* **365,** 810–816
6. Archer, S. J., Vinson, V. K., Pollard, T. D., and Torchia, D. A. (1994) *FEBS Lett.* **337,** 145–151
7. Mahoney, N. M., Janmey, P. A., and Almo, S. C. (1997) *Nat. Struct. Biol.* **4,** 953–960
8. Mahoney, N. M., Rozwarski, D. A., Fedorov, E., Fedorov, A. A., and Almo, S. C. (1999) *Nat. Struct. Biol.* **6,** 666–671
9. Chang, F., Drubin, D., and Nurse, P. (1997) *J. Cell Biol.* **137,** 169–182
10. Kovar, D. R., Kuhn, J. R., Tichy, A. L., and Pollard, T. D. (2003) *J. Cell Biol.* **161,** 875–887
11. Balasubramanian, M. K., Hirani, B. R., Burke, J. D., and Gould, K. L. (1994) *J. Cell Biol.* **125,** 1289–1301
12. Goode, B. L., and Eck, M. J. (2007) *Annu. Rev. Biochem.* **76,** 593–627
13. Pruyne, D., Evangelista, M., Yang, C., Bi, E., Zigmond, S., Bretscher, A., and Boone, C. (2002) *Science* **297,** 612–615
14. Sagot, I., Rodal, A. A., Moseley, J., Goode, B. L., and Pellman, D. (2002) *Nat. Cell Biol.* **4,** 626–631
15. Kovar, D. R., Harris, E. S., Mahaffy, R., Higgs, H. N., and Pollard, T. D. (2006) *Cell* **124,** 423–435
16. Vavylonis, D., Kovar, D. R., O'Shaughnessy, B., and Pollard, T. D. (2006) *Mol. Cell* **21,** 455–466
17. Romero, S., Le Clainche, C., Didry, D., Egile, C., Pantaloni, D., and Carlier, M. F. (2004) *Cell* **119,** 419–429
18. Kaiser, D. A., Goldschmidt-Clermont, P. J., Levine, B. A., and Pollard, T. D. (1989) *Cell Motil. Cytoskeleton* **14,** 251–262
19. Almo, S. C., Pollard, T. D., Way, M., and Lattman, E. E. (1994) *J. Mol. Biol.* **236,** 950–952
20. Spudich, J. A., and Watt, S. (1971) *J. Biol. Chem.* **246,** 4866–4871
21. Pollard, T. D. (1984) *J. Cell Biol.* **99,** 769–777
22. Otwinowski, Z., and Minor, W. (1997) *Methods Enzymol.* **276,** 307–326
23. Perrakis, A., Morris, R., and Lamzin, V. S. (1999) *Nat. Struct. Biol.* **6,** 458–463
24. Murshudov, G. N., Vagin, A. A., and Dodson, E. J. (1997) *Acta Crystallogr. Sect. D Biol. Crystallogr.* **53,** 240–255
25. Emsley, P., and Cowtan, K. (2004) *Acta Crystallogr. Sect. D Biol. Crystallogr.* **60,** 2126–2132
26. Winn, M. D., Isupov, M. N., and Murshudov, G. N. (2001) *Acta Crystallogr. Sect. D Biol. Crystallogr.* **57,** 122–133
27. Painter, J., and Merritt, E. A. (2006) *Acta Crystallogr. Sect. D Biol. Crystal-*

[9] N. S. Younger and D. R. Kovar, manuscript in preparation.

logr. **62,** 439–450
28. Laskowski, R. A., Moss, D. S., and Thornton, J. M. (1993) *J. Mol. Biol.* **231,** 1049–1067
29. Delano, W. L. (2002) *PYMOL*, Delano Scientific, LLC, Palo Alto, CA
30. Jones, T. A., Zou, J. Y., Cowan, S. W., and Kjeldgaard, M. (1991) *Acta Crystallogr. Sect. A* **47,** 110–119
31. Ostrander, D. B., Ernst, E. G., Lavoie, T. B., and Gorman, J. A. (1999) *Eur. J. Biochem.* **262,** 26–35
32. Christensen, H. E. M., Ramachandran, S., Tan, C. T., Surana, U., Dong, C. H., and Chua, N. H. (1996) *Plant J.* **10,** 269–279
33. Perelroizen, I., Didry, D., Christensen, H., Chua, N. H., and Carlier, M. F. (1996) *J. Biol. Chem.* **271,** 12302–12309
34. Wen, K.-K., McKane, M., Houtman, J. C. D., and Rubenstein, P. A. (2008) *J. Biol. Chem.* **283,** 9444–9453
35. Eads, J. C., Mahoney, N. M., Vorobiev, S., Bresnick, A. R., Wen, K. K., Rubenstein, P. A., Haarer, B. K., and Almo, S. C. (1998) *Biochemistry* **37,** 11171–11181
36. Liu, S., Fedorov, A. A., Pollard, T. D., Lattman, E. E., Almo, S. C., and Magnus, K. A. (1998) *Struct. Biol.* **123,** 22–29
37. Perelroizen, I., Carlier, M., and Pantaloni, D. (1995) *J. Biol. Chem.* **270,** 1501–1508
38. Perelroizen, I., Marchand, J. B., Blanchoin, L., Didry, D., and Carlier, M. F. (1994) *Biochemistry* **33,** 8472–8478
39. Petrella, E. C., Machesky, L. M., Kaiser, D. A., and Pollard, T. D. (1996) *Biochemistry* **35,** 16535–16543
40. Skare, P., and Karlsson, R. (2002) *FEBS Lett.* **522,** 119–124
41. Suetsugu, S., Miki, H., and Takenawa, T. (1998) *EMBO J.* **17,** 6516–6526
42. Mimuro, H., Suzuki, T., Suetsugu, S., Miki, H., Takenawa, T., and Sasakawa, C. (2000) *J. Biol. Chem.* **275,** 28893–28901
43. Metzler, W. J., Bell, A. J., Ernst, E., Lavoie, T. B., and Mueller, L. (1994) *J. Biol. Chem.* **269,** 4620–4625
44. Wittenmayer, N., Jandrig, B., Rothkegel, M., Schlüter, K., Arnold, W., Haensch, W., Scherneck, S., and Jockusch, B. M. (2004) *Mol. Biol. Cell* **15,** 1600–1608
45. Fraser, H. B., Hirsh, A. E., Steinmetz, L. M., Scharfe, C., and Feldman, M. W. (2002) *Science* **296,** 750–752
46. Dominguez, R. (2004) *Trends Biochem. Sci.* **29,** 572–578
47. Paul, A. S., and Pollard, T. D. (2008) *Curr. Biol.* **18,** 9–19